Articles

Ni(II)-Doped $CsCdBrCl_2$: Variation of Spectral and Structural Properties via Mixed-Halide Coordination

S. R. Lüthi* and M. J. Riley

Department of Chemistry, University of Queensland, St. Lucia, QLD 4072, Australia

Received August 8, 2000

The mixed-halide compound $CsCdBrCl_2$ is studied by X-ray diffraction and by using the Ni(II) ion as an optical probe. Low-temperature absorption, luminescence, and EXFAS spectra of the Ni(II) impurity are recorded. The structure of $CsCdBrCl_2$ is shown to consist of corner-sharing $[Cd_3X_{12}]^{6-}$ trimers. Each trimer has a structure of three face-sharing octahedra $Cl_3CdX_3CdX_3CdCl_3$ where X has an equal probability of being a Br^- or a Cl^- ion. This equal occupancy on the bridging halide positions occurs over the whole crystal rather than within each $[Cd_3X_{12}]^{6-}$ trimer unit. Optical spectroscopy shows that the Ni(II) ion exists in all possible $[NiBr_xCl_{6-x}]^{4-}$ isomeric forms ($x = 0, 1, ..., 6$). The energy of the $^3A_{2g} \rightarrow {}^1A_{1g}$ transition is a *linear* function of x, due to the change in inter-electron repulsion through the differing covalencies of the ligand compositions. The energy of this transition can be varied over 2750 cm^{-1}. The inhomogeneous broadening that results from the halide disorder is discussed from the point of view of the variation of ligand-field strength and inter-electron repulsion. A model including a differential nephelauxetic effect is required to explain the energies of the ligand-field states.

Introduction

Over recent years, Ni(II)-doped materials have received considerable attention in optical spectroscopic research because of their ability to show multiple luminescence transitions.[1] There is a major interest in Ni(II) as an active center in the development of tunable lasers in the near-infrared spectral range, at about 1.5 μm. This wavelength has important applications in measuring techniques and optical data transmission in glass fibers.[2,3] A broad-band emission around 1.5 μm stems from the $^3T_{2g} \rightarrow {}^3A_{2g}$ transition from the first excited to the electronic ground state of the Ni(II) ion in octahedral coordination. The energy of this transition is sensitive to the strength of the ligand field[4,5] and thus can be varied over a wide range by changing the host lattice.[2,4] Studies on the influence of chemical variation on the spectroscopic properties of a material also provide insight into the mechanisms that control properties such as the radiative and nonradiative relaxation rates. This insight allows the spectroscopic properties to be improved for optical devices. To date, the main disadvantage of Ni(II)-doped compounds for use as tunable near-infrared laser sources has been the thermal quenching of the $^3T_{2g} \rightarrow {}^3A_{2g}$ luminescence at higher temperatures.[2,6] Lasing has been restricted to temperatures below −30 and 0 °C for continuous-wave and pulsed operations, respectively.[2,7,8]

Interest in the spectroscopic properties of Ni(II), however, is not restricted to the $^3T_{2g} \rightarrow {}^3A_{2g}$ luminescent transition. The Ni(II) ion is one of the rare transition-metal ions that show emission from higher excited states when doped into different inorganic host materials.[1,5,9−11] Depending on the ligand-field strength of the chosen host lattice, the $^1T_{2g} \rightarrow {}^3A_{2g}$, $^1T_{2g} \rightarrow {}^3T_{2g}$, and $^1T_{2g} \rightarrow {}^3T_{1g}$ luminescent transitions cover the green to near-infrared spectral range. This higher excited-state luminescence is of interest not only for the application of Ni(II)-doped compounds as phosphors and laser materials but also for the application of transition-metal/rare-earth-metal codoped systems with Ni(II) as a sensitizer for enhanced rare-earth-metal emission.[12]

The energies of the Ni(II) excited states leads to a competition of different radiative and nonradiative processes. Oetliker et al.[13] have shown that efficient cross-relaxation and multiion energy-transfer processes in Ni(II)-doped $CsCdCl_3$ can lead to nonlinear optical behavior called an "excitation avalanche". This phenomenon results in up-conversion in energy and has been observed in a number of rare-earth-metal-doped compounds

(1) Iverson, M. V.; Sibley, W. A. *J. Lumiun.* **1979**, *20*, 311−324.
(2) Koetke, J. Ph.D. Thesis, University of Hamburg.
(3) Alcala, R.; Gonzalez, J. C.; Villacampa, B.; Alonso, P. J. *J. Lumin.* **1991**, *48/49*, 569−573.
(4) Liehr A. D.; Ballhausen, C. J. *Ann. Phys.* **1959**, *6*, 134−155.
(5) De Viry, D.; Tercier, N.; Denis, J. P.; Blanzat, B.; Pellé, F. *J Chem. Phys.* **1992**, *97*, 2263−2270.
(6) Elejalde, M. J.; Balda, R.; Fernandez, J. *J. Phys. IV* **1994**, *C4*, 411−414.
(7) Moulton P. F.; Mooradian, A. *Springer Ser. Opt. Sci.* **1979**, *21*, 584−589.
(8) Moulton, P. F. In *Laser Handbook*, 5th ed.; Bass, Stitch, Eds.; North-Holland Publishing Co.: Amsterdam, 1979; pp 257−266.
(9) May, P. S.; Güdel, H. U. *Chem. Phys. Lett.* **1989**, *164*, 612−616.
(10) May, P. S.; Güdel, H. U. *J Lumin.* **1990**, *46*, 277−290.
(11) May, P. S.; Güdel, H. U. *J. Chem. Phys.* **1991**, *95*, 6343−6354.
(12) Lüthi, S. R.; Riley, M. J. Unpublished results.
(13) Oetliker, U.; Riley, M. J.; May, P. S.; Güdel, H. U. *J. Lumin.* **1992**, *53*, 553−556.

10.1021/ic000899l CCC: $20.00
Published on Web 12/15/2000

(Pr^{3+}:$LaCl_3$, Pr^{3+}:$LaBr_3$, Sm^{3+}:$LaBr_3$, Nd^{3+}:$YLiF_4$),[14] but Ni(II):$CsCdCl_3$ is the only species providing an example of an excitation avalanche in a transition-metal system. The study and optimization of these processes could lead to the development of Ni(II)-based materials with nonlinear optical properties for applications in optical devices.

In this work, we demonstrate the influence of chemical variation on the spectroscopic properties of Ni(II) on a finer scale than is normally possible. The synthesis of the novel *mixed*-halide compound $CsCdBrCl_2$ offers the possibility to study the effect of partial exchange of halide counterions on the energy levels of the Ni(II) d−d excitations. The observed spectral properties are compared with those of the structurally related Ni(II)-doped $CsCdBr_3$ and $CsCdCl_3$ compounds and are simulated with calculations. Chemical substitution of one-third of the chloride ligands with bromide in $CsCdBrCl_2$ does not result in a simple additive effect expected for chemical variation along the halide series. The structural changes have a strong impact on the spectroscopic properties. We can distinguish various effects of chemical substitution on the basis of interelectron repulsions, ligand-field strengths, bond lengths, and Ni(II) site symmetries all within the single Ni(II):$CsCdBrCl_2$ system. Only the study of Ni(II) in glasses would offer a comparable or finer grid for varying the chemical environment; however, in glasses, the advantage of Ni(II) in a well-defined host is lost.

Experimental Section

Synthesis. The synthesis, crystal growth, and preparation of samples for spectroscopic measurements of the ternary metal halides $CsCdX_3$ (X = Cl, Br) are dictated by the hygroscopic nature of the compounds and their binary starting materials CsX and CdX_2. Under ambient conditions, the binary and ternary halides react with water to form hydrated halides, resulting in crystal decomposition. For this reason, the preparations of the pure $CsCdX_3$ and the mixed $CsCdBrCl_2$ were carried out in a dry nitrogen atmosphere and special purification procedures for the starting materials were applied.

The ternary metal halides $CsCdBrCl_2$, $CsCdBr_3$ and $CsCdCl_3$ were synthesized from a congruently melting phase which forms from the reaction of the binary halides CsX and CdX_2. Water-free binary halides of high purity are the key to high-quality $CsCdX_3$ crystals for spectroscopic applications. The commercially available starting materials CsX, CdX_2, and NiX_2 of >99.9% purity were dried under vacuum at 250 °C for 3 h and then sublimed to remove traces of hydrocarbons and other impurities. During crystal growth, hydrocarbons decompose to form carbon particles that have been shown to adversely affect the crystal quality.[15] For sublimation, the powdered starting materials were transferred into a quartz glass ampule, which was evacuated to $<10^{-4}$ mbar. The temperature was increased to slightly above the melting point of the respective compound, and the sublimation was carried out over 1 day.

Stoichiometric mixtures of CsX, CdX_2, and NiX_2 were used to grow crystals of $CsCdBr_3$, $CsCdBrCl_2$, and $CsCdCl_3$ with 5% of the Cd(II) replaced by Ni(II). After transference of the mixtures to quartz glass ampules and evacuation to $<10^{-5}$ mbar, the ampules were sealed. Prior to the crystal growth, the fused ampules were placed into the Bridgman furnace in an upright position and heated for 2 h to give completely clear melts. The temperature was chosen to be approximately 50 °C above the melting temperature of the lowest melting component, i.e., 450 °C for $CsCdBr_3$ and 550 °C for $CsCdCl_3$. In the case of the mixed halide $CsCdBrCl_2$, a clear melt was obtained after heating to 550 °C. The temperature gradient and furnace speed were chosen such that the growth period was typically 7−10 days. The resulting 5% Ni(II):$CsCdBr_3$ single crystals showed a slight concentration gradient for Ni(II), obvious from the change in intensity of the-typical red color for Ni(II)-doped halides along the growth direction. The crystals preferentially cleaved perpendicular to the crystallographic *c* axis. The Ni(II):$CsCdBrCl_2$ single crystals also showed a slight concentration gradient but cleaved like Ni(II):$CsCdCl_3$, preferentially along the *c* axis. No concentration gradient was found for the Ni(II):$CsCdCl_3$ crystals. Crystals were chosen such that the actual concentration of Ni(II) in each doped compound was close to *5%*.

For the spectroscopic measurements, single crystals of the three compounds were oriented under a microscope with crossed polarizers. The samples were sealed into epoxy resin, cut, and polished with aluminum oxide (Al_2O_3) powders of decreasing size down to 0.3 μm, to allow for σ-, π-, and α-polarized experiments.

The crystallographic structure of the novel compound $CsCdBrCl_2$ was determined on a single-crystal X-ray diffractometer (Nonius-Enraf CAD 4) at room temperature. The quality of the already known compounds $CsCdBr_3$ and $CsCdCl_3$ was checked with the same instrument. For the structure determination, single crystals with dimensions of approximately 100 × 100 × 300 μm were used.

Spectroscopy. Overview absorption spectra of all three compounds were recorded on a Cary 17D spectrometer (Varian). The samples were cooled with a closed-cycle cryostat (Leybold-Heraeus ROK) down to 10 K. The high-resolution absorption experiments were performed on a single-beam absorption instrument, equipped with a 150 W halogen light source. The light was dispersed with a Spex 1701 single monochromator equipped with a 1200 line/mm grating, blazed at 500 nm (for spectra in the range 300−800 nm), or a 600 line/mm grating, blazed at 1.6 μm (for spectra in the range 800−2500 nm). The light was focused on the masked sample, and the transmitted light was detected with either an S-20 photomultiplier tube (300−800 nm) or a liquid N_2 cooled InSb diode (800−2500 nm). The sample absorbance *A* was then calculated from the transmitted intensities with (I_{sample}) and without (I_0) the sample: $A = \log(I_0/I_{sample})$. The spectra were plotted in units of extinction coefficient ϵ (l mol^{-1} cm^{-1}) per energy interval *E* (cm^{-1}).

The luminescence spectra were obtained by exciting the samples with an Ar^+ or a Kr^+ ion laser in single-line configuration (Spectra Physics model 165). The sample luminescence was dispersed with a Spex 1401 double monochromator equipped with 1200 line/mm gratings blazed at 500 nm and detected with a photomultiplier tube (RCA 31034A) in the photon-counting mode. The signal was amplified with a preamplifier (Stanford SR445) and acquired with a photon-counting system (Stanford SR400). The measured luminescence spectra $S_{exp}(\lambda)$ were corrected for the response of the detection system using a calibrated blackbody source $B_{exp}(\lambda)$ (tungsten band lamp with a color temperature of 2590 K). The spectrum of a theoretical blackbody $B_{th}(\lambda)$ was calculated from the expression[16]

$$B_{th}(\lambda) = 2\pi c\lambda^{-4}[\exp(hc/\lambda kT) - 1]^{-1} \quad (1)$$

where the symbols have their usual meanings. The corrected luminescence spectra $S_{cor}(\lambda)$ were obtained from the measured spectra $S_{exp}(\lambda)$ according to

$$S_{cor}(\lambda) = S_{exp}(\lambda)\, B_{th}(\lambda)/B_{exp}(\lambda) \quad (2)$$

Transformation of the recorded spectra into units of photon flux J_E (cm^{-1} s) per energy interval *E* (cm^{-1}) was performed according to the procedures described by Ejder.[16]

For the high-resolution absorption and luminescence measurements, the samples were cooled to 5 K using a helium flow-tube cryostat.

EXAFS Experiments. All X-ray absorption experiments were performed at the Australian National Beam Facility (ANBF) on the bending magnet beamline B20 at the KEK Photon Factory, Tsukuba,

(14) (a) Chivian, J. S.; Case, W. E.; Eden, D. D. *Appl. Phys. Lett.* **1979**, *35*, 124−125. (b) Krausutsky, N. J. *J. Appl. Phys.* **1983**, *54*, 1261−1267. (c) Koch, M. E.; Case, W. E. *Adv. Laser Sci.* **1986**, *1*, 142−144. (d) Kueny, A. W.; Case, W. E.; Koch, M. E. *J. Opt. Soc. Am. B* **1989**, *6*, 639−642. (e) Lenth, W.; Macfarlane, R. M. *J. Lumin.* **1990**, *45*, 346−350. (f) Case, W. E.; Koch, M. E.; Kueny, A. W. *J Lumin.* **1990**, *45*, 351−353.

(15) Krämer, K. W. Private communication.

(16) Ejder, E. *J. Opt. Soc. Am.* **1969**, *59*, 223−224.

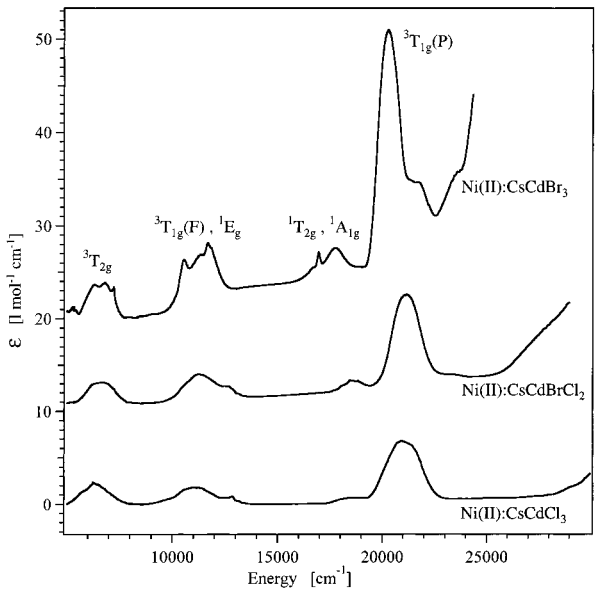

Figure 1. Unpolarized overview absorption spectra of $CsCdBr_3$, $CsCdBrCl_2$, and $CsCdCl_3$ doped with 5% Ni(II), recorded at 10 K. The transitions are labeled for Ni(II) in octahedral symmetry.

Japan. Samples of $CsCdBr_3$, $CsCdBrCl_2$, and $CsCdCl_3$ doped with 5% Ni(II) for the EXAFS analysis were prepared by pressing finely ground powders into an aluminum sample holder (1 mm thick; 10 mm diameter hole in center) and held in place with Kapton tape windows. During the measurement of the X-ray absorption spectra, the 2.5 GeV storage ring delivered a current between 400 and 200 mA. The data were collected in the fluorescence mode with a standard Lytle detector. Three scans of the X-ray absorption spectra were recorded at room temperature for each compound. The EXAFS measurements were acquired in three stages: (i) the smooth, featureless preedge region (8100−8300 eV), with 10 eV steps; (ii) the absorption edge (8300−8370 eV), where the largest changes are expected, with 0.5 eV steps; and (iii) the region exhibiting more slowly varying EXAFS oscillations (8370−9345 eV), with uniform steps of 0.5 Å^{-1} in reciprocal space. All experiments were performed on the Ni K-edge, and the energies were calibrated to the first inflection point of the Ni K-edge being assigned as 8333 eV.

Data processing and evaluation were performed with the XFIT software.[17] The calculated EXAFS data were fitted to the observed k^3-weighted data over the k range 2.5−12 Å^{-1}, and the r range was restricted to the region of interest 0.0−6.0 Å. All atoms within 5.0 Å were included in a number of models which were then fitted to the experimental spectra using single-scattering theory, FEFF4.[18,19] The quality of the fit was monitored by means of the residual R, which was calculated using

$$R = (\chi^2/\chi_0^2)^{1/2} \quad (3)$$

where χ^2 is the quantity minimized in the refinement and χ_0^2 is the value of χ^2 when the calculated EXAFS is uniformly 0.

Results

Figure 1 shows the unpolarized overview absorption spectra of $CsCdBr_3$, $CsCdBrCl_2$, and $CsCdCl_3$ doped with 5% Ni(II), recorded at 10 K. The assignment of the d−d energy levels for Ni(II) in the novel compound $CsCdBrCl_2$ is straightforward.

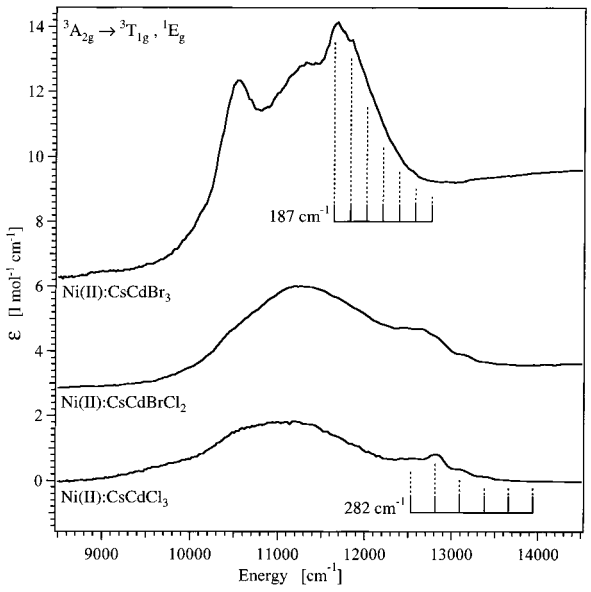

Figure 2. Unpolarized absorption spectra of the $^3A_{2g} \rightarrow {}^3T_{1g}$ (F), ^1E_g transitions for $CsCdBr_3$, $CsCdBrCl_2$, and $CsCdCl_3$ doped with 5% Ni(II), recorded at 10 K. The spectral resolution is 2 nm. For $CsCdBr_3$ and $CsCdCl_3$, the first members of a vibrational progression with separation energies of 187 and 282 cm^{-1} are indicated. The vibronic structure is less evident for $CsCdBr_3$ at 10 K but has been verified with absorption experiments at 1.6 K not shown here.

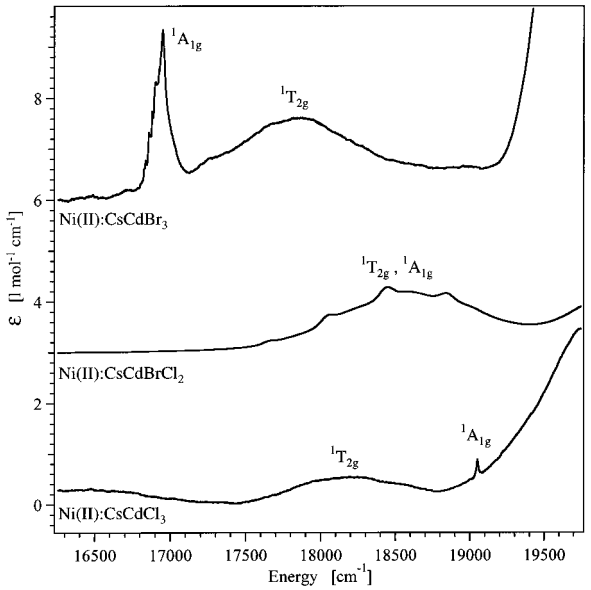

Figure 3. Unpolarized high-resolution absorption spectra of the $^3A_{2g} \rightarrow {}^1T_{2g}$, $^1A_{1g}$ transitions for $CsCdBr_3$, $CsCdBrCl_2$, and $CsCdCl_3$ doped with 5% Ni(II), recorded at 5 K. The spectral resolution is 0.1 nm.

Assignments were not made for transitions above 22 500 cm^{-1}, as the low-lying charge-transfer bands in this spectral range obscure them. The transitions are labeled for Ni(II) in octahedral symmetry. Figure 2 is an enlargement of the $^3A_{2g} \rightarrow {}^3T_{1g}$, ^1E_g spectral region with a resolution of 2 nm, recorded at 10 K. The high-energy part of the band system shows a vibronic progression for all three compounds; the first members of the progression and the separation energy are indicated for Ni(II)-doped $CsCdBr_3$ and $CsCdCl_3$, respectively. Figure 3 shows the region of the $^3A_{2g} \rightarrow {}^1T_{2g}$, $^1A_{2g}$ transitions with a spectral resolution of 0.1 nm, recorded at 5 K.

The experimental energies for the transitions assigned in Figures 1−3 are summarized in Table 1. For all experimentally

(17) Ellis, P. J.; Freeman, H. C. *J. Synchrotron Radiat.* **1995**, *2*, 190−195.
(18) Rehr, J. J.; Mustre de Leon, J.; Zabinsky, S. I.; Albers, R. C. *J. Am. Chem. Soc.* **1991**, *113*, 5135−5140.
(19) Mustre de Leon, J.; Rehr, J. J.; Zabinsky, S. I.; Albers, R. C. *Phys. Rev. B* **1991**, *44*, 4146−4156.

Table 1. Experimental Energy Levels and Absorption Transition Intensities[a]

	Ni(II):$CsCdBr_3$		Ni(II):$CsCdBrCl_2$		Ni(II):$CsCdCl_3$	
state	energy (cm^{-1})	$10^{-5}f_{osc}$	energy (cm^{-1})	$10^{-5}f_{osc}$	energy (cm^{-1})	$10^{-5}f_{osc}$
$^3A_{2g}$	0		0		0	
$^3T_{2g}$	6 600	1.382	6 600	1.469	6 100	0.907
$^3T_{1g}$ (F)	11 200	2.916	11 400	2.376	10 750	1.296
^1E_g	10 600				12 700	
$^1T_{2g}$	17 650	1.015	18 500	0.346	18 100	0.129
$^1A_{1g}$	16 950	0.151			19 060	0.004
$^3T_{1g}$(P)	20 350	10.80	21 150	6.588	20 400	4.450

[a] The energies represent the band maxima of the respective transitions in absorption. The oscillator strengths, f_{osc}, are averaged over both σ- and π-polarizations and are dimensionless.

Table 2. Parameters and Calculated Energy Levels for Ni(II) in $CsCdBr_3$, $CsCdBrCl_2$, and $CsCdCl_3$[a]

	Ni(II):$CsCdBr_3$	Ni(II):$CsCdBrCl_2$	Ni(II):$CsCdCl_3$
B	751	819	794
C	2679	3084	3174
Δ	6791	6727	6329
σ_{dev}	218	78	322

[a] The Ni(II) site symmetry was assumed to be O_h, and spin−orbit coupling was ignored. *B* and *C* are the Racah parameters, and Δ is the octahedral ligand-field splitting. All values are given in cm^{-1}. σ_{dev} is the rms standard deviation for the calculated energy levels.

resolved and assigned transitions, the experimentally determined oscillator strengths, f_{osc}, are given. These were calculated from the integral under the absorption curve using the formula[20]

$$f_{osc} = \frac{10^3 mc^2 \ln(10)}{N_A \pi e^2} \int \epsilon(\nu)\, d\nu \qquad (4)$$

where the symbols have their usual meanings and the integration runs over the whole absorption profile, with the experimental data plotted in ϵ ($1\ mol^{-1}\ cm^{-1}$) versus wavenumber ν (cm^{-1}). The experimentally assigned d−d transitions (Table 1) were used to fit the ligand-field parameters. The fitted parameters are given in Table 2 for Ni(II) in octahedral symmetry without spin−orbit coupling.

Figure 4 shows the calculated energies of selected excited states of Ni(II) as a function of (a) the Racah parameter *B* and (b) the octahedral ligand-field splitting parameter Δ. For Figure 4a, the ligand-field parameter Δ was set to 6600 cm^{-1} and a fixed *C*/*B* ratio of 3.8 was used. For Figure 4b, the Racah parameters *B* and *C* were set to 800 and 3040 cm^{-1}, respectively. The values were selected to be representative for Ni(II) doped into the three host lattices discussed here (see Table 2). The explicit expressions for the energies of these transitions are well-known.[21]

To more thoroughly understand the differences found in the spectroscopic properties of Ni(II) doped into $CsCdBr_3$, $CsCdBrCl_2$, and $CsCdCl_3$ and to compare them with other halides, calculations were also performed for Ni(II) in other hosts with the experimental data taken from literature. From this comparison, good agreement was found between the data for Ni(II)-doped $CsCdBr_3$ and $CsCdCl_3$ and the general trend for Ni(II) in halide host materials. Figure 5 shows the unpolarized

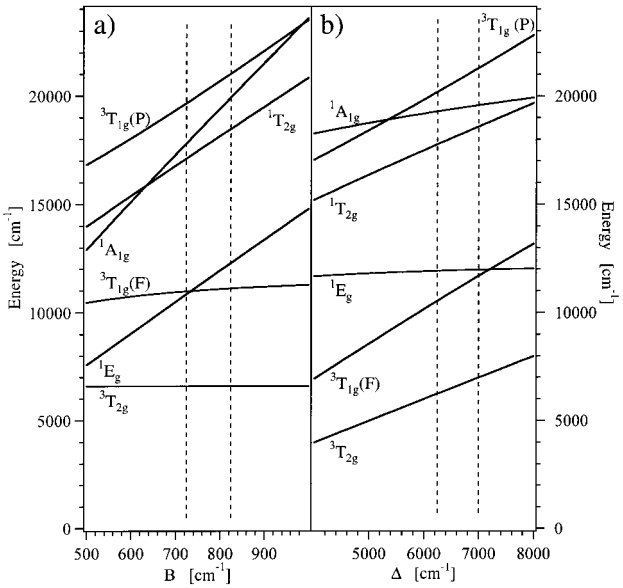

Figure 4. Calculated energies of some excited d states for the d^8 electronic configuration of Ni(II) as a function of (a) Racah parameter *B* and (b) ligand-field splitting Δ. The calculations are for Ni(II) in O_h symmetry. For the calculations in (a), the *C*/*B* ratio was fixed to $C = 3.8B$ and $\Delta = 6600\ cm^{-1}$; for (b) *B* and *C* were set to $B = 800\ cm^{-1}$ and $C = 3040\ cm^{-1}$. These values were chosen to be representative of the situations found in Ni(II)-doped $CsCdBr_3$, $CsCdBrCl_2$, and $CsCdCl_3$. The dashed vertical lines indicate the regions appropriate to $[NiX_6]^{4-}$ halide complexes.

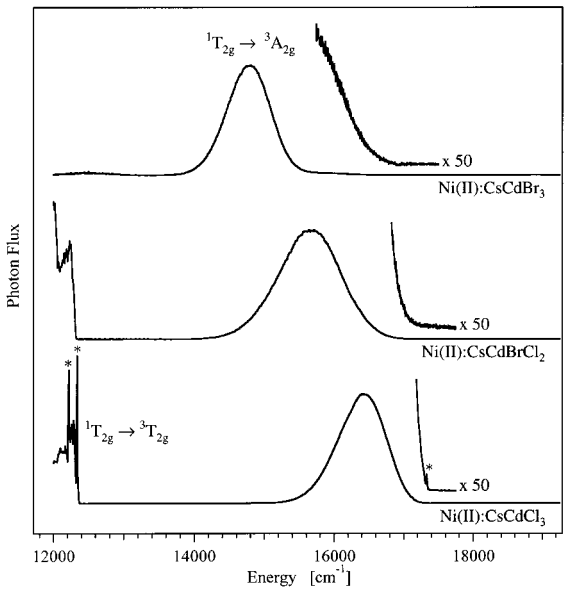

Figure 5. Unpolarized luminescence spectra of $CsCdBr_3$, $CsCdBrCl_2$, and $CsCdCl_3$ doped with 5% Ni(II), recorded at 10 K, after excitation at 488 nm with an Ar^+ laser. The spectral resolution is 0.15 nm. The transitions are labeled for Ni(II) in O_h symmetry. The transitions marked with an asterisk are identified as electronic origins.[11] No electronic origins could be identified for $CsCdBr_3$ and $CsCdBrCl_2$ doped with *5%* Ni(II).

luminescence spectra of Ni(II)-doped $CsCdBr_3$, $CsCdBrCl_2$, and $CsCdCl_3$ recorded at 10 K, with a spectral resolution of 0.15 nm.

To our knowledge, $CsCdBrCl_2$ was synthesized and characterized for the first time in this study. The relevant crystallographic data are summarized and compared to those for the related compounds $CsCdBr_3$ and $CsCdCl_3$ in Table 3. The

(20) Ballhausen, C. J. *Molecular Electronic Structure of Transition Metal Compounds*; McGraw-Hill: London, 1979.
(21) Sugano, S.; Tanabe, Y.; Kamimura, H. *Multiplets of Transition Metal Ions in Crystals*; Academic Press: New York, 1970.

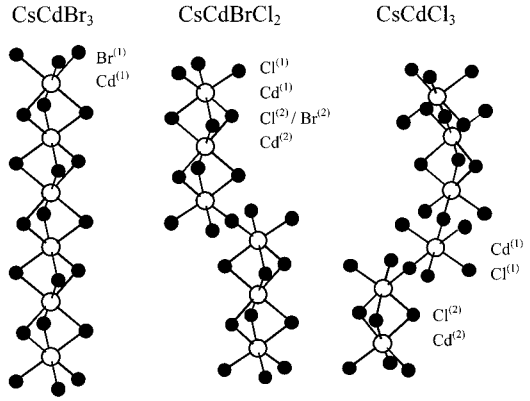

Figure 6. Partial views of the crystal structures for $CsCdBr_3$, $CsCdBrCl_2$, and $CsCdCl_3$ showing the connectivities of the $[CdX_6]^{4-}$ units (X = Br, Cl). The crystallographic *c* axis runs vertically for all three systems. The Cs^+ ions have been omitted for clarity. Relevant crystallographic data for the crystal structures are given in Table 3.

Table 3. Crystallographic Data for $CsCdBr_3$, $CsCdBrCl_2$, and $CsCdCl_3$ Doped with 5% Ni(II), Recorded at 295 K[a]

	Ni(II):$CsCdBr_3$	Ni(II):$CsCdBrCl_2$	Ni(II):$CsCdCl_3$
space group	$P6_3/mmc$	$R\bar{3}m$	$P6_3/mmc$
$a = b$, c (Å)	7.663(1), 6.702(2)	7.4984(6), 28.679(2)	7.395(1), 18.426(8)
$\alpha = \beta$, γ (deg)	90, 120	90, 120	90, 120
Z	2	9	6
$Cd^{(1)}$ site symmetry	D_{3d}	C_{3v}	D_{3d}
$Cd^{(2)}$ site symmetry		D_{3d}	C_{3v}
$Cd^{(1)}-X^{(1)}$ (Å)	2.764(1)	2.6067(4)	2.604(8)
$Cd^{(1)}-X^{(2)}$ (Å)		2.7273(10)	
$Cd^{(2)}-X^{(1)}$ (Å)			2.581(8)
$Cd^{(2)}-X^{(2)}$ (Å)		2.7006(9)	2.573(8)
$\phi_{Cd^{(1)}X^{(1)}}$ (deg)	+2.1	−1.4	−0.9
$\phi_{cd^{(1)}X^{(2)}}$ (deg)		+2.9	
$\phi_{Cd^{(2)}X^{(1)}}$ (deg)			−0.5
$\phi_{Cd^{(2)}X^{(2)}}$ (deg)		+2.2	+5.0

[a] The angle ϕ is the deviation of the angle between the Cd−X bond and the trigonal axis from the octahedral value of 54.74°. Positive values of ϕ imply a trigonal elongation. The labeling of $Cd^{(1)}$, $Cd^{(2)}$, $X^{(1)}$, and $X^{(2)}$ is defined in Figure 6. The structural data given for Ni(II):$CsCdBr_3$ and Ni(II):$CsCdCl_3$ have been determined under the same conditions as those for Ni(II):$CsCdBrCl_2$ and are in good agreement with the published structures.[30,31] The values in parentheses are the experimental errors in the last digits.

Table 4. Comparison of Average Cd−X (X = Cl, Br) Bond Lengths Obtained from the Crystallographic Data with Ni−X Bond Lengths Extracted from EXAFS[a]

	Ni(II):$CsCdBr_3$	Ni(II):$CsCdBrCl_2$	Ni(II):$CsCdCl_3$
		X-ray Data	
$(Cd-X)_{av}$	2.764	2.6782	2.586
		EXAFS Data	
Ni−Br	2.539	2.547	
Ni−Cl		2.377	2.412

[a] The EXAFS data for Ni(II):$CsCdBrCl_2$ were fitted to a $[NiBr_2Cl_4]^{4-}$ complex. All values are given in angstroms.

connectivities of the $[CdX_6]^{4-}$ octahedra in all three lattices are shown in Figure 6. A comparison of the average Cd−X bond lengths from the X-ray crystal structures and the Ni−X bond lengths in these host lattices determined from EXAFS experiments at 295 K is given in Table 4. In fitting the EXAFS data, we investigated two models and refined both against the

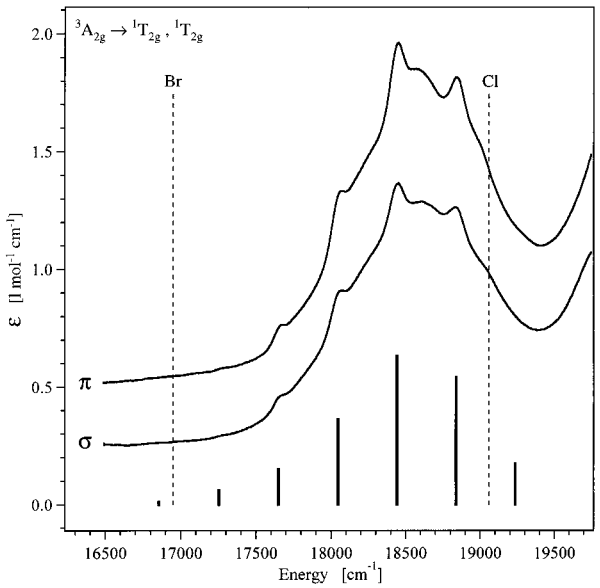

Figure 7. Comparison of experimental transition intensities in the $^3A_{2g} \rightarrow {}^1T_{2g}$, $^1A_{1g}$ spectral range for Ni(II):$CsCdBrCl_2$ and calculated intensities for a statistical distribution of Br^-/Cl^- in the face-sharing positions of Ni(II):$CsCdBrCl_2$ over the whole lattice (Table 6). The experimental absorption spectra were recorded in σ- and π-polarizations at 5 K with a resolution of 0.08 nm. The dashed lines indicate the energies of the $^3A_{2g} \rightarrow {}^1A_{2g}$ transitions in $CsCdBr_3$ and $CsCdCl_3$. The calculated intensities for the $[CdBr_xCl_{6-x}]^{4-}$ species in $CsCdBrCl_2$ are separated by 397 cm^{-1}.

experimental spectra. These were (i) a model where there was only one unique Ni−X bond length for a particular ligand type and, (ii) a model where the lengths of opposite bonds were allowed to vary. In all cases, the second model refined to the same structural parameters as the first model.

Figure 7 compares the σ- and π-polarized absorption spectra for the $^3A_{2g} \rightarrow {}^1T_{2g}$, $^1A_{1g}$ region, with the calculated intensities for the $^3A_{2g} \rightarrow {}^1A_{1g}$ transition assuming a statistical distribution of Br^-/Cl^- ligands within the face-sharing halide positions of the $[NiX_6]^{4-}$ octahedra in Ni(II):$CsCdBrCl_2$. The calculated transition intensities are located at positions separated by 397 cm^{-1} to fit the structure observed in the $^3A_{2g} \rightarrow {}^1T_{2g}$, $^1A_{1g}$ transitions. It is assumed that the transitions are shifted to lower energy as more Br^- ions are coordinated to the Ni(II) ion. The experimental spectra were recorded at 5 K with a spectral resolution of 0.08 nm. Figure 7 also indicates, with dashed lines, the experimental energies of the $^3A_{2g} \rightarrow {}^1A_{1g}$ transitions in Ni(II):$CsCdBr_3$ and Ni(II):$CsCdCl_3$.

Energy level calculations for Ni(II):$CsCdBrCl_2$ using a differential nephelauxetic model were performed *including* the $^1A_{1g}$ state in the fitting procedure at the experimentally observed energies (see Figures 2, 3, and 7). This is in contrast to the calculations for Ni(II):$CsCdBr_3$ and Ni(II):$CsCdBrCl_2$ (Table 2), where this state was *excluded* from the fitting procedure. In the case of Ni(II):$CsCdBr_3$, the normal ligand-field model cannot account for the experimentally observed ordering of the $^1A_{1g}$ and $^1T_{2g}$ states, and for Ni(II):$CsCdBrCl_2$, the $^1A_{1g}$ state cannot be attributed to one single energy (as discussed below). Figure 8 illustrates the trends for the parameter values (Figure 8a) and the excited-state energies (Figure 8b) from these calculations and compares them to the experimentally observed energies. The final values of the fitted parameters and the energies of the relevant excited d states $^3T_{1g}(F)$, ^1E_g, $^1A_{1g}$, and $^1T_{2g}$ are given. The Racah parameters *B* and *C* were held fixed at their free-ion values (B = 1041 cm^{-1}, C = 4831 cm^{-1}) in the

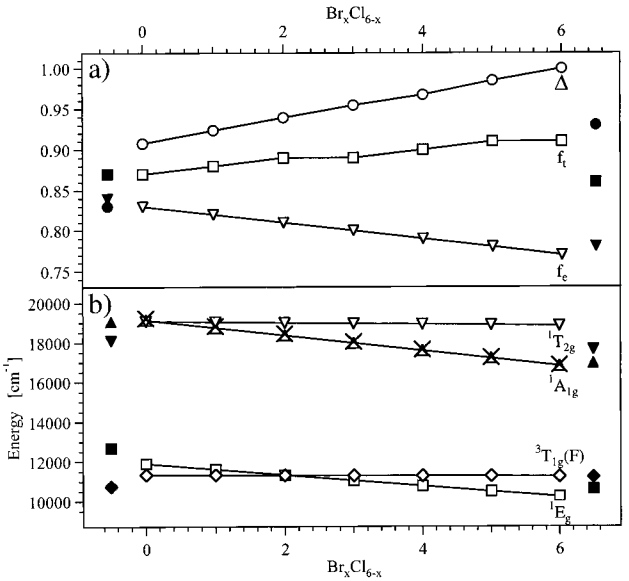

Figure 8. Graphic presentation of the trends in the parameter values and calculated energy levels for Ni(II):$CsCdBrCl_2$ using the nephelauxetic model. (a) The parameter values f_e, f_t, and Δ are shown as a function of the Br^-:Cl^- ratio in the $[NiBr_xCl_{6-x}]^{4-}$ coordination site ($x = 0, ..., 6$). For Δ, relative values are given, with $\Delta = 1$ chosen for $[NiBr_6]^{4-}$. The parameter values for Ni(II):$CsCdBr_3$ and Ni(II):$CsCdCl_3$ are shown for comparison (full symbols). (b) The excited-state energies of some selected states are shown as a function of the Br^-:Cl^- ratio. The experimentally assigned energies of the $^1A_{1g}$ state for Ni(II):$CsCdBrCl_2$ are indicated ($\times$) as well as the respective experimental energies for the pure halides Ni(II):$CsCdBr_3$ and Ni(II):$CsCdCl_3$ (full symbols).

calculations with the covalency factors f_e and f_t; and Δ is shown relative to its value for $[NiBr_6]^{4-}$.

Discussion

Energy Level Structure. The 10 K overview absorption spectra of Ni(II) in $CsCdBr_3$ and $CsCdCl_3$ reveal the expected general red shift for most of the d−d transitions between the chloride and the bromide host lattices (Figure 1). The spectrum of Ni(II) in the mixed compound $CsCdBrCl_2$, however, does not fit into this trend. The absorption band maxima in this compound are *blue* shifted with respect to those of the chloride. The energy shift observed between the pure bromide and the pure chloride hosts fits well into the general trend observed along the halide series of transition-metal ions.[22] This red shift along the series F → Cl → Br → I mainly results from a superposition of two effects: (i) the nephelauxetic effect,[23−25] where the inter-electron repulsion of the metal ion valence electrons is reduced because of the increased metal−ligand covalency and ligand polarizability along the halide series; (ii) the decrease of the ligand-field strength due to the decreasing σ-antibonding strength, which is a consequence of the increase in the average metal−ligand bond length of the host lattice along the halide series. For transition-metal ions, these two effects are of comparable magnitude and predominate over the spin−orbit coupling. For this reason, our study is focused on the inter-electron repulsion and ligand-field interactions and we neglect the spin−orbit coupling in the model calculations.[22]

Energy level calculations for Ni(II) in $CsCdBr_3$ and $CsCdCl_3$ reproduce the expected red shift (Table 2). The trend in the fitted Racah parameters also agrees with energy level calculations performed for Ni(II) in a variety of halide host materials, using the same approximations as for the calculations for Ni(II) in $CsCdBr_3$, $CsCdBrCl_2$, and $CsCdCl_3$. The change in the Racah parameters is approximately 20% between fluorides and chlorides and 10% between chlorides and bromides. This is in good agreement with the trend observed for the Ni−X (X = F, Cl, Br, I) bond lengths, which increase more dramatically between fluorides and chlorides than between chlorides and bromides. The increasing bond length along the halide series is a convenient measure of the polarizability and the covalency of a metal−halide bond and hence of the nephelauxetic effect.[26] Between the bromides and iodides the relative increase in the average bond length is again larger than that between chlorides and bromides and the effect on the inter-electron repulsion is also expected to be larger.

The energy calculations for Ni(II):$CsCdBrCl_2$ were fitted to the experimentally observed absorption bands (Table 1). The calculated energy levels are higher than those for Ni(II):$CsCdBr_3$ and Ni(II):$CsCdCl_3$, and the Racah parameters *B* and *C* are larger than those for the pure bromide and chloride (Table 2). This discrepancy is not consistent with the Cd−X bond lengths in the three host lattices (Tables 3 and 4). The average Cd−X bond lengths show the expected increase from the pure chloride to the mixed bromide−chloride to the pure bromide, which suggests a general red shift along the series $CsCdCl_3$ → $CsCdBrCl_2$ → $CsCdBr_3$. From the EXAFS experiments performed on the title compounds, however, it is evident that the actual Ni−X bond lengths are more comparable to those in pure nickel halide systems than to the Cd−X bond lengths in the host compounds (Tables 3 and 4).

A general decrease in the ligand-field strength Δ along the halide series F → Cl → Br → I is found from the energy level calculations for Ni(II) in various halide host materials. The trend, however, is not as clear-cut as in the case of the inter-electron repulsion. From the calculations we can extract average decreases of ∼5% between fluorides and chlorides and ∼2.5% between chlorides and bromides. The trend in the ligand-field strength and the nephelauxetic effect, as discussed above, is only strictly valid for transition-metal ions with exactly the same ligand coordination symmetry. Changes in the symmetry of the ligand coordination have an effect on the ligand-field strength as well as the different ligand types within the halide series. It is not surprising, therefore, that the ligand-field strength for Ni(II) in host materials with the same halide ion but with slightly different coordination symmetries varies almost as much as that for Ni(II) in host materials with comparable coordination symmetries but with different halide ligands. Comparison among $CsCdBr_3$, $CsCdBrCl_2$, and $CsCdCl_3$ indicates the strongest effective ligand field is apparently that for Ni(II) in $CsCdBr_3$, followed by that for Ni(II) in $CsCdBrCl_2$, and the weakest effective ligand field is that for Ni(II) in $CsCdCl_3$ (Table 2). This is unexpected, as one would expect Δ to be larger for the Cl ligands. This will be rationalized below in a more sophisticated model, which is able to describe covalency differences between e_g and t_{2g} orbitals, referred to as the differential

(22) (a) Jørgensen, C. K. *Modern Aspects of Ligand Field Theory*; North-Holland Publishing Co.: Amsterdam, 1971. (b) Griffith, J. S. *The Theory of Transition-Metal Ions*; Cambridge University Press: Cambridge, U.K., 1971. (c) Gerloch, M.; Slade, R. C. *Ligand-Field Parameters*; Cambridge University Press: Cambridge, U.K., 1973. (d) Lever, A. B. P. *Inorganic Electronic Spectroscopy*, 2nd ed.; Elsevier: Amsterdam, 1984.
(23) Jørgensen, C. K. *Prog. Inorg. Chem.* **1962**, *4*, 73−124.
(24) König, E. *Struct. Bonding* **1970**, *7*, 175−212.
(25) König, E. *Z. Naturforsch.* **1971**, *27B*, 1−6.
(26) Gao, F.; Zhang, S. *J. Phys. Chem. Solids* **1997**, *58*, 1991−1994.

nephelauxetic effect. Figure 4 shows the d−d excitation energies as a function of Racah parameter B and ligand-field strength Δ. The excited-state energies depend on the variations of B and Δ to different extents. The energies of the $^3A_{2g} \rightarrow {}^1E_g$, $^1A_{1g}$ transitions are more sensitive to B and C, whereas the energies of the $^3A_{2g} \rightarrow {}^3T_{1g}(F)$, $^1T_{2g}$ transitions are more sensitive to Δ.

Fitting the experimentally determined energy level structure with a model in which the Ni(II) ion has octahedral site symmetry places the excited $^1A_{1g}$ state above the $^1T_{2g}$ state for all three compounds (Figure 4). This is also true for calculations using the same model for all other hosts used for comparison purposes in this study. The calculations are in agreement with the experimental assignment for $CsCdCl_3$[27] but not with that for Ni(II):$CsCdBr_3$ (Figure 3). Attempts to calculate the energy level structure for Ni(II) such that the $^1A_{1g}$ state lies below the $^1T_{2g}$ state lead to major discrepancies in the energies of most of the other excited states and to parameter values that lack physical meaning. Taking into account the actual host lattice distortions, $O_h \rightarrow C_{3v}$ for Ni(II) in $CsCdCl_3$ and $O_h \rightarrow D_{3d}$ for Ni(II) in $CsCdBr_3$, as well as spin−orbit coupling, energy level calculations showed that the $^1A_{1g}$ and $^1T_{2g}$ states strongly mix. The assignment of the $^1T_{2g}$, $^1A_{1g}$ region for Ni(II) in $CsCdBrCl_2$ is discussed in detail below.

A general red shift of the band maxima of the Ni(II) $^1T_{2g} \rightarrow {}^3A_{2g}$ luminescence transition at 10 K is observed within the series $CsCdCl_3 \rightarrow CsCdBrCl_2 \rightarrow CsCdBr_3$ (Figure 5). This is a clear indication that the band maxima in absorption are a superposition of species all of which are seen. In luminescence, only a minority of Ni(II) ions with halide coordinations that fit into the expected chemical trend along the halide series are probed. The excitation energy absorbed from the system is transferred to these energetically low-lying Ni(II) ions, from where it is emitted. From the luminescence spectra, we can observe the electronic origin of the $^1T_{2g} \rightarrow {}^3A_{2g}$ transition for Ni(II) in $CsCdCl_3$ at 17 326 cm^{-1} [27] and estimate the origins for Ni(II) in $CsCdBrCl_2$ and $CsCdBr_3$ to be at ∼17 050 and ∼16 650 cm^{-1}, respectively. The lack of an observed electronic origin for Ni(II) in $CsCdBr_3$ and $CsCdBrCl_2$ is also suggestive that in these host lattices Ni(II) does not occupy a single site. The luminescence transition $^1T_{2g} \rightarrow {}^3T_{2g}$ can be observed for the $CsCdBrCl_2$ and $CsCdCl_3$ compounds. Only a very small red shift is observed on going from $CsCdCl_3$ to $CsCdBrCl_2$. The electronic origins of this transition can be assigned to 12 337 and 12 217 cm^{-1} for $CsCdCl_3$.[11] No electronic origins are observed for this transition in $CsCdBrCl_2$. For Ni(II):$CsCdBr_3$, the $^1T_{2g} \rightarrow {}^3T_{2g}$ luminescence is situated around ∼11 250 cm^{-1} and was not detected in our experiments.[5]

Transition Intensities. A general increase in the Ni(II) absorption transition intensities along the series $CsCdCl_3 \rightarrow CsCdBrCl_2 \rightarrow CsCdBr_3$ is evident from the absorption spectra at 10 K (Figure 1, Table 1). This is due to the lowering in energy of the intense charge-transfer bands along this series. Lower energy charge-transfer states are mixed more efficiently into the Laporte-forbidden d−d transitions by perturbations such as vibronic coupling and noncentrosymmetric ligand fields for the different Ni(II) coordination.

The red shift of the Ni(II) $^1T_{2g} \rightarrow {}^3A_{2g}$ luminescence at 10 K along the series $CsCdCl_3 \rightarrow CsCdBrCl_2 \rightarrow CsCdBr_3$ accompanies a strong decrease of the luminescence intensity by approximately 2 orders of magnitude along $CsCdCl_3 \rightarrow CsCdBrCl_2 \rightarrow CsCdBr_3$. This obvious reduction of the luminescence intensity can be explained by the decreasing energy gap between the excited states, which strongly favors nonradiative transition via multiphonon relaxation versus radiative transitions between neighboring d−d states. Increasing the temperature toward 295 K increases the multiphonon relaxation and thus leads to a reduction of the luminescence yield for all systems.[11] At 295 K, a very broad, weak luminescence band could be observed for Ni(II)-doped $CsCdCl_3$, situated around 15 500 cm^{-1}, but no emission could be detected for the other two compounds. Another mechanism reducing the luminescence yield of the systems is cross-relaxation. The energy level structure of Ni(II) offers the following cross-relaxation pathways after excitation in the blue-green spectral range: $^1T_{2g}$, $^3A_{2g} \rightarrow {}^3T_{2g}$, $^3T_{1g}$ and $^1T_{2g}$, $^3A_{2g} \rightarrow {}^3T_{1g}$, $^3T_{2g}$.[9] This mechanism becomes more efficient at higher Ni(II) concentrations, as increased concentrations lead to more efficient energy transfer between Ni(II) ions. Cross-relaxation is a key process for the excitation avalanche observed in Ni(II)-doped $CsCdCl_3$.[13] No attempt was made to investigate either cross-relaxation or excitation avalanche in Ni(II)-doped $CsCdBrCl_2$.

Structure of $CsCdBrCl_2$ and Ni(II) Coordination in Ni(II):$CsCdBrCl_2$. The X-ray structure of $CsCdBrCl_2$ shows that the compound crystallizes in the hexagonal space group $P6_3/mmc$ and is isomorphous with $CsMnCl_3$.[28] This novel compound is one of the rare *mixed* halides.[29] The relevant crystallographic data are listed in Table 3, and the characteristic structural features are shown in Figure 6. The full refinement for the structures of Ni(II)-doped and pure $CsCdBrCl_2$ single crystals will be presented elsewhere. The compound consists of trimers of face-sharing $[CdX_6]^{4-}$ octahedra (X = Br, Cl). The terminal $[Cd^{(1)}X_6]^{4-}$ octahedra of the three $Cd^{(1)}$−$Cd^{(2)}$−$Cd^{(1)}$ face-sharing octahedra join corners with neighboring trimers of face-sharing octahedra. The corner-sharing halide positions bound to the terminal $Cd^{(1)}$ are in all cases occupied by chloride ions only ($Cl^{(1)}$). The face-sharing halide positions, however, are occupied by equal amounts of Br^- and Cl^- ions ($Br^{(2)}$, $Cl^{(2)}$). From the crystallographic data, it is not possible to conclude whether there is a fixed repeating arrangement or simply a random distribution of the $Br^{(2)}$ and $Cl^{(2)}$ ions to these positions throughout the crystal lattice.

The structure of $CsCdBrCl_2$ is closely related to those of $CsCdBr_3$ and $CsCdCl_3$. $CsCdBr_3$ consists of linear chains of face-sharing $[CdBr_6]^{4-}$ octahedra parallel to the crystallographic c axis,[30] and $CsCdCl_3$ consists of pairs of face-sharing $[Cd^{(2)}Cl_6]^{4-}$ octahedra connected via a corner-sharing single $[Cd^{(1)}Cl_6]^{4-}$ octahedron to the next pair of face-sharing octahedra ($Cd^{(2)}$).[31] For comparison, the structural features of $CsCdBr_3$ and $CsCdCl_3$ are also listed in Table 3 and shown in Figure 6. Ni(II) substitutes for Cd(II) when doped into these three lattices. The Cd(II) site symmetry is C_{3v} or D_{3d} for the different sites in $CsCdBr_3$, $CsCdBrCl_2$, and $CsCdCl_3$, with small departures from strict O_h symmetry in all cases (Table 3). In what follows, we define ϕ as the deviation of the angle a Cd−X bond makes with the c axis from the octahedral value. In $CsCdBrCl_2$, two-thirds of the Cd(II) sites have C_{3v} symmetry ($Cd^{(1)}$). In these sites, the $[CdX_6]^{4-}$ octahedra show trigonal compression along

(27) Oetliker, U.; Riley, M. J.; Güdel, H. U. *J. Lumin.* **1995**, *63*, 63−73.

(28) McPherson, G. L.; Kistenmacher, T. J.; Stucky, G. D. *J. Chem. Phys.* **1970**, *52*, 815−824.

(29) (a) Witteveen, H. T.; Reedijk, J. *Solid State Commun.* **1973**, *12*, 397−400. (b) Witteveen, H. T.; Jongejan, D. L.; Brandwijk, V. *Mater. Res. Bull.* **1974**, *9*, 345−352. (c) Brixner, L. H.; Chen, H. Y.; Foris, C. M. *J. Solid State Chem.* **1981**, *40*, 336−343. (d) Butler, S. E.; Smith, P. W.; Stranger, R.; Grey, I. E. *Inorg. Chem.* **1986**, *25*, 4375−4378.

(30) McPherson, G. L.; McPherson, A. M.; Atwood, J. L. *J. Phys. Chem. Solids* **1980**, *41*, 495−499.

(31) Chang, J. R.; McPherson, G. L.; Atwood, J. L. *Inorg. Chem.* **1975**, *14*, 3079−3085.

the *c* axis of $\phi = -1.4°$ for the $Cd^{(1)}-Cl^{(1)}$ bonds which are corner-sharing to another octahedron and a trigonal elongation of $\phi = +2.9°$ for the $Cd^{(1)}-X^{(2)}$ bond connecting to the face-sharing $[CdX_6]^{4-}$ octahedron ($Cd^{(2)}$). The other one-third of the Cd(II) sites have D_{3d} symmetry ($Cd^{(2)}$), with a trigonal elongation for the $Cd^{(2)}-X^{(2)}$ bond along the *c* axis of $\phi = +2.2°$. $CsCdBr_3$ has only one Cd(II) site, which has D_{3d} symmetry with a trigonal elongation of $\phi = +2.1°$. The $CsCdCl_3$ host lattice again has two Cd(II) sites. The single, corner-sharing $[CdCl_6]^{4-}$ octahedron ($Cd^{(1)}$) has D_{3d} symmetry with a slight trigonal compression of $\phi = -0.9°$. The face-sharing $[CdCl_6]^{4-}$ octahedra ($Cd^{(2)}$) have C_{3v} symmetry with a trigonal compression of $\phi = -0.5°$ for the $Cd^{(2)}-Cl^{(1)}$ bonds with the corner-sharing $Cl^{(1)}$ and a larger trigonal elongation of $\phi = +5.0°$ for the $Cd^{(2)}-Cl^{(2)}$ bonds connecting to the neighboring face-sharing $[CdCl_6]^{4-}$ octahedron ($Cd^{(2)}$). The Cd−Cd distances within the face-sharing $[Cd_2X_9]^{5-}$ units are 3.351, 3.3274, and 3.328 Å and the trigonal elongations are $\phi = +2.1$, $+2.2$, and $+5.0°$ for the bridging ligands in $CsCdBr_3$, $CsCdBrCl_2$, and $CsCdCl_3$, respectively. A considerable interaction between metal ions substituting for Cd(II) in adjacent positions can be expected. Such interactions can lead to interesting magnetic phenomena[30−32] but also to nonlinear optical behavior due to excited-state interactions within dimers of active centers.[13,33]

Several attempts were made to synthesize Ni(II):$CsCdBr_2Cl$ from a stoichiometric mixture of CsX, CdX_2, and NiX_2 (X = Cl, Br) in a Bridgman furnace. However, a compound with this stoichiometry does not appear to be stable; only polycrystalline substances resulted. Powder X-ray diffraction of the products revealed traces of $CsCdCl_3$ and $CsCdBr_3$ as well as many unidentified species. It is likely that the formation of a stable phase with this composition is not possible, but we note that, in the $CsScBr_xCl_{3-x}$ system,[34] stable compounds with $x = 0$, 1, 2, 3 were obtained.

Ni−X Bond Lengths in $CsCdBr_3$, $CsCdBrCl_2$, and $CsCdCl_3$. When Ni−X bond lengths (X = F, Cl, Br, I) in pure nickel compounds are compared to the Cd−X bond lengths for the related cadmium compounds, the Ni−X bonds are on average ∼9% shorter. The EXAFS study on Ni(II) doped in small concentrations (1−5%) into the $CsCdBr_3$ and $CsCdCl_3$ host lattices yielded average Ni−X distances of 2.539 and 2.412 Å, respectively. For Ni(II):$CsCdBrCl_2$, values of 2.377 and 2.547 Å were found for Ni−Cl and Ni−Br bond lengths, respectively. These values are comparable to the Ni−X bond lengths in the related pure nickel compounds, which are ∼2.547 and ∼2.407 Å for bromides and chlorides, respectively. They differ considerably from the Cd−X bond lengths in the respective cadmium host lattices, which are ∼2.779 and ∼2.634 Å for Cd−Br and Cd−Cl, respectively.

The Ni−X bond lengths extracted from the EXAFS data are average values only. No attempts were made to fully resolve values for all *different* site geometries of Ni(II) present in the three compounds. The two simple models used to fit the experimental data all yielded *R* values on the order of ∼25%. For the Ni(II):$CsCdBrCl_2$ system, it will be shown that the $[NiBr_xCl_{6-x}]^{4-}$ complex varies in halide composition from $x = 0$ to 6. Clearly, fitting the EXAFS spectra to a single $[NiBr_2Cl_4]^{4-}$ species is a gross approximation, although this is the most numerous of the seven possible stoichiometric species.

The average Ni−Cl bond extracted from the EXAFS data for $CsCdBrCl_2$ is slightly shorter than the average value found for the Ni−Cl bond in $CsCdCl_3$. While it is expected that the various $[NiBr_xCl_{6-x}]^{4-}$ species will adopt their own equilibrium geometries, they may experience a smaller effective host cavity in $CsCdBrCl_2$ than that experienced by $[NiCl_6]^{4-}$ in $CsCdCl_3$. This could explain the observed trend in the optical spectra of Ni(II):$CsCdBrCl_2$ and $CsCdCl_3$, as discussed in. above. The shorter Ni−X bond length is expected to increase the ligand-field strength and the inter-electron repulsion between the d electrons, leading to a blue shift of the spectrum.

Investigation of the $^3A_{2g} \rightarrow {}^1T_{2g}$, A_{1g} Spectral Region. The $^3A_{2g} \rightarrow {}^1T_{2g}$, $^1A_{1g}$ spectral region shows pronounced differences among the three compounds (Figure 3). For Ni(II):$CsCdCl_3$, the $^3A_{2g} \rightarrow {}^1A_{1g}$ transition is a sharp weak feature on the high-energy side of the broad $^3A_{2g} \rightarrow {}^1T_{2g}$ transition. This energy ordering is also found in the energy level calculations. The polarization dependence (strong in π polarization; weak in σ and α polarizations) indicates that this is a spin-forbidden electric-dipole-allowed transition. This polarization behavior implies that the Ni(II) ion preferentially occupies the C_{3v} site in $CsCdCl_3$,[27] which is in agreement with EPR experiments.[31] For Ni(II):$CsCdBr_3$, the $^3A_{2g} \rightarrow {}^1A_{1g}$ transition is assigned to the sharp, relatively intense feature on the low-energy side of the $^3A_{2g} \rightarrow {}^1T_{2g}$ transition.[5] This is in contrast to the energy level calculations, which predict the $^1A_{1g}$ state to again be above the $^1T_{2g}$ excited state. This transition does not show pronounced polarization dependence. Furthermore, the $^3A_{2g} \rightarrow {}^1A_{1g}$ transition of Ni(II):$CsCdBr_3$ shows very rich structure at temperatures below 40 K. This is unexpected for a transition between states to the same electron configuration and to an excited state without spin and angular degeneracy. It is our intention to investigate this observation in a subsequent paper.

The $^3A_{2g} \rightarrow {}^1T_{2g}$, $^1A_{1g}$ transitions of $CsCdBrCl_2$ are characterized by a broad band, assigned to $^3A_{2g} \rightarrow {}^1T_{2g}$, superimposed with seven weak sharper features, separated by approximately 397 cm^{-1} from each other and spread over the $^3A_{2g} \rightarrow {}^1T_{2g}$ transition (Figure 7). This energy interval (397 cm^{-1}) is much larger than the totally symmetric vibration energies for either $[NiBr_6]^{4-}$ (∼185 cm^{-1})[35] or $[NiCl_6]^{4-}$ (264 cm^{-1}).[36] Further, the intensity distribution does not follow a Franck−Condon pattern and one would not expect the $^1A_{1g}$ state to be strongly coupled to the a_{1g} totally symmetric coordinate (Figure 4). This implies that some other mechanism is responsible for this structure.

The X-ray structure refinement for Ni(II):$CsCdBrCl_2$ indicates Cl^- ions in the corner-sharing positions of the $Cd^{(1)}$ octahedra and a random distribution of Cl^- and Br^- ions with equal probability for the face-sharing positions within each $[Cd_3X_{12}]^{6-}$ unit. The $CsCdBrCl_2$ compound could be more accurately written as CsCd(Br/Cl)(Br/Cl)Cl where (Br/Cl) indicates equal probability of occupancy in the face-sharing positions. There are two ways in which this can occur: an equal occupancy of the face-sharing positions (i) *within* each $[Cd_3X_{l2}]^{6-}$ trimer and (ii) *distributed* over the whole lattice. These two cases are indistinguishable by crystallography. The first case leads to 20 possible structural isomers:

(32) Ackerman, J.; Holt, E. M.; Holt, S. L. *J. Solid State Chem.* **1974**, *9*, 279−296.
(33) Hehlen, M. P.; Kuditcher, A.; Rand, S. C.; Lüthi, S. R. *Phys. Rev. Lett.* **1999**, *82*, 3050−3053.
(34) Meyer, G.; Corbett, J. D. *Inorg. Chem.* **1981**, *20*, 2627−2631.
(35) Nakamoto, K. *Infitared and Raman Spectra of Inorganic and Coordination Compounds*, 5th ed.; Wiley-Interscience: New York, 1997.
(36) Akiyama, K.; Morioka, Y.; Nakagawa, I. *Bull. Chem. Soc. Jpn.* **1978**, *51*, 103−107.

$$2 \times \textit{fac}\text{-}Cl_3CdCl_3CdBr_3CdCl_3$$

$$6 \times \textit{fac}\text{-}Cl_3CdBrCl_2CdBr_2ClCdCl_3$$

$$12 \times \textit{mer}\text{-}Cl_3CdBr_2ClCdBrCl_2CdCl_3$$

where *fac* and *mer* refer to the coordination of the central $Cd^{(2)}$ ion. There are 60 ($=3 \times 6!/3!^2$) possible ways of arranging three Br^- and three Cl^- ions in the face-sharing positions. This results in nine nonequivalent coordination geometries of the $[CdBr_xCl_{6-x}]^{4-}$ complex as shown in Table 5.

In this case of random distribution *within each trimer*, each $Cd^{(2)}$ is coordinated by exactly three Br^- and three Cl^- ions. Nine of these arrangements are nonequivalent if their symmetry is determined by the number and relative disposition of the ligand types; i.e., we neglect the small distortions which distinguish the symmetry of the $Cd^{(1)}$ and $Cd^{(2)}$ sites. Of the 60 possible arrangements, two are for $[CdCl_6]^{4-}$ coordination with octahedral symmetry. A total of 18 sites have $[CdBrCl_5]^{4-}$ coordination with tetragonal symmetry. There are another 18 sites having *cis*-$[CdBr_2Cl_4]^{4-}$ coordination of different but also tetragonal symmetry. A total of 22 sites have $[CdBr_3Cl_3]^{4-}$ coordination, 10 with *fac*-$[CdBr_3Cl_3]^{4-}$ trigonal symmetry and 12 with *mer*-$[CdBr_3Cl_3]^{4-}$ orthorhombic symmetry. Within this approximation, it would be expected that there are five sites having different types of ligand fields with a ratio of 2:18:18:10:12 and that the spectra thus would consist of a superposition of signals for species experiencing these different ligand fields in the given ratios. The corresponding transition intensities, however, would not necessarily be expected to follow these ratios, as in some sites the transitions would be far more electric dipole allowed than others.

Alternatively, the equal probability of face-sharing positions could be statistically spread *over the whole crystal*. In this second case, the Cd(II) sites range from $[CdBr_6]^{4-}$ to $[CdCl_6]$.$^{4-}$ The 192 ($=3 \times 2^6$) possible arrangements result in 29 different nonequivalent sites, as shown in Table 6. Without going into the details of the symmetry of these sites, clearly one expects a superposition of spectra, each of whose intensities could be independent of the statistical number in each site.

Summing over structural isomers in Table 6, the distribution for the total number of different $[CdBr_xCl_{6-x}]^{4-}$ coordinations is given by expressions 5a,b and the last column of Table 6.

$$N_x = \frac{6!}{(6-x)!x!} + \frac{2^4 3!}{(3-x)!x!} \qquad x \le 3 \qquad (5a)$$

$$N_x = \frac{6!}{(6-x)!x!} \qquad x > 3 \qquad (5b)$$

The observed structure in the $^3A_{2g} \rightarrow {}^1T_{2g}$, $^1A_{1g}$ spectral range can best be explained with this second model.

From eqs 5a,b, a random distribution with a 1:1 ratio of Cl^- and Br^- ions for all bridging halide positions within the $CsCdBrCl_2$ crystal gives rise to a statistical distribution for $[CdBr_xCl_{6-x}]^{4-}$ octahedra of 17:54:63:36:15:6:1 as x is varied from 0 to 6. This is very close to the distribution observed for the $^3A_{2g} \rightarrow {}^1A_{1g}$ transition intensities shown in Figure 7. It has already been shown that this transition is particularly sensitive to inter-electron repulsion but rather insensitive to the ligand field. If we assume that each substitution of a Cl^- with a Br^- ion results in the observed 397 cm^{-1} red shift due to the reduction in the inter-electron repulsion, then we see a very close correspondence between the statistical distribution of the number of Br^- ions and the experimental observations. This is *regardless of the ligand fields* of the individual isomers.

Table 5. Numbers of Different Possible $[CdBr_xCl_{6-x}]^{4-}$ Sites (x = 0, ..., 3) for Equal Occupancy of the Face-Sharing Positions *within Each* $[Cd_3X_{12}]^{6-}$ *Trimer*[a]

x	$Cd^{(1)}$	$Cd^{(2)}$	Σ
0	2 (C_{3v})		2
1	6 (C_s) 12 (C_1)		18
2	6 (C_s) 12 (C_1)		18
3	2 (C_{3v})	2 (C_{3v}) 6 (C_s) 12 (C_1)	22
			60

[a] $Cd^{(1)}$ and $Cd^{(2)}$ are the terminal and central Cd(II) ions, respectively. The site symmetries of the $[CdBr_xCl_{6-x}]^{4-}$ complexes are given in parentheses. The last column lists the sum of Cd(II) ions for the same approximate coordination symmetry, as discussed in the text.

Table 6. Numbers of Different Possible $[CdBr_xCl_{6-x}]^{4-}$ Sites for Equal Occupancy of the Face-Sharing Positions of $CsCdBrCl_2$ *over the Whole Lattice* (x = 0, ..., 6)[a]

x	$Cd^{(2)}$	$Cd^{(1)}$	[neighbors]	Σ
0	1 (D_{3d})	2 (C_{3v})	$[Cd^{(2)}Cl_6]$	
		6 (C_s)	$[Cd^{(2)}BrCl_5]$	17
		6 (C_s)	$[Cd^{(2)}Br_2Cl_4]$	
		2 (C_{3v})	$[Cd^{(2)}Br_3Cl_3]$	
1	6 (C_s)	6 (C_s)	$[Cd^{(2)}BrCl_5]$	
		18 ($6C_s + 12C_1$)	$[Cd^{(2)}Br_2Cl_4]$	54
		18 ($6C_s + 12C_1$)	$[Cd^{(2)}Br_3Cl_3]$	
		6 (C_s)	$[Cd^{(2)}Br_4Cl_2]$	
2	3 (C_{2h})	6 (C_s)	$[Cd^{(2)}Br_2Cl_4]$	
	6 (C_2)	18 ($6C_s + 12C_1$)	$[Cd^{(2)}Br_3Cl_3]$	63
	6 (C_s)	18 ($6C_s + 12C_1$)	$[Cd^{(2)}Br_4Cl_2]$	
		6 (C_s)	$[Cd^{(2)}Br_5Cl]$	
3	2 (C_{3v})	2 (C_{3v})	$[Cd^{(2)}Br_3Cl_3]$	
	6 (C_2)	6 (C_s)	$[Cd^{(2)}Br_4Cl_2]$	36
	12 (C_1)	6 (C_s)	$[Cd^{(2)}Br_5Cl]$	
		2 (C_{3v})	$[Cd^{(2)}Br_6]$	
4	3 (C_{2h})			
	6 (C_2)			15
	6 (C_s)			
5	6 (C_s)			
				6
6	1 (D_{3d})			1
				192

[a] $Cd^{(1)}$ and $Cd^{(2)}$ are the terminal and central Cd(II) ions, respectively. The site symmetries of the $[CdBr_xCl_{6-x}]^{4-}$ complexes are given in parentheses. For $Cd^{(1)}$, the halide coordination of the neighboring $Cd^{(2)}$ is indicated in square brackets. The last column lists the sum of Cd(II) ions for a given halide coordination.

For a pure chloride coordination ($x = 0$), the $^3A_{2g} \rightarrow {}^1A_{1g}$ transition is predicted to be at 19 236 cm^{-1}, compared to 19 060 cm^{-1} found for Ni(II):$CsCdCl_3$. For the pure bromide coordination ($x = 6$), the $^3A_{2g} \rightarrow {}^1A_{1g}$ transition is predicted to be at 16 855 cm^{-1}, close to the position of the transition observed for Ni(II):$CsCdBr_3$ (16 950 cm^{-1}). We conclude that, for this transition, the change in the inter-electron repulsion due to the difference in the number of Br^-/Cl^- ions within the Ni(II) coordination sphere, or stoichiometry, predominates over the effect of the actual ligand-field strength or coordination symmetry. In some respects, this is quite surprising. While the $^3A_{2g} \rightarrow {}^1A_{1g}$ transition is essentially independent of ligand-field strength, the intensity of the transition would still be expected to depend on the symmetry of the complex. We conclude that the electric-dipole contribution is not dominant for the overall

transition intensity; otherwise, different geometries would lead to different dipole moments and result in a different intensity distribution.

The excited-state energies of the Ni(II) d^8 electronic configuration can be expressed as a function of the Racah parameters B and C and the ligand-field strength Δ. The effect of the variation of B and Δ on the energies of the excited Ni(II) d states is shown in Figure 4. The energy of the $^1A_{1g}$ excited state has a stronger dependence on B than does the energy of the $^1T_{2g}$ state. The opposite trend is found for the dependence of the excited-state energies on Δ. The energy of the $^1A_{1g}$ state depends less critically on variations in Δ than does the energy of the $^1T_{2g}$ state. This is why the $^3A_{2g} \rightarrow {}^1A_{1g}$ structures and transition intensities follow a simple statistical distribution for the number, rather than the arrangement, of halide ions in the Ni(II) coordination sphere.

The fact that the $^3A_{2g} \rightarrow {}^1A_{1g}$ absorption bands for the different $[NiBr_xCl_{6-x}]^{4-}$ ($x = 0$, ..., 6) species in $CsCdBrCl_2$ still have a full width half-maximum (FWHM) of $\sim$100 cm^{-1} at 5 K, as well as the lack of an electronic origin in the $^1T_{2g} \rightarrow {}^3A_{2g}$ luminescence transition, indicates that, apart from the seven different halide coordinations, there may be considerable disorder in the Ni(II) lattice sites. This is expected because of the number of possible nonequivalent isomers for each $[NiBr_xCl_{6-x}]^{4-}$ stoichiometry. The absence of polarization behavior in the transitions is additional indication of different Ni(II) environments with different transition-intensity mechanisms contributing to the overall $^3A_{2g} \rightarrow {}^1T_{2g}$, $^1A_{1g}$ absorption band shape.

Similar observations are also made for Ni(II)-doped $CsCdBr_3$. The $^3A_{2g} \rightarrow {}^1A_{1g}$ transition also has a FWHM of $\sim$100 cm^{-1} at 5 K. However, the transition shows an unexpected, rich structure at temperatures below 40 K. Again, the $^1T_{2g} \rightarrow {}^3A_{2g}$ luminescence transition shows no evidence of an electronic origin. The fact that the $CsCdBr_3$ host lattice has only one Cd(II) site (D_{3d}), together with the unusually large intensity of the $^3A_{2g} \rightarrow {}^1A_{1g}$ transition and the discrepancy between the Cd−Br and Ni−Br bond lengths found in X-ray and EXAFS studies, suggests that the Ni(II) ions in $CsCdBr_3$ may be subject to a distortion. The situation in Ni(II):$CsCdCl_3$ is different. While this lattice has two Cd(II) sites, the $^3A_{2g} \rightarrow {}^1A_{1g}$ transition is much sharper, having FWHM's of only 23.5 cm^{-1} with 5% dopant concentration (Figure 3) and 14.1 cm^{-1} with 0.25% dopant concentration (not shown). The polarization dependence of the transition and the observation of an electronic origin for the $^1T_{2g} \rightarrow {}^3A_{2g}$ luminescence transition (Figure 5) both support the hypothesis of Ni(II) in a single site with C_{3v} site symmetry. This is in agreement with EPR[31] and excited-state emission studies.[27]

Differential Nephelauxetic Effect. From the discussion in the previous sections, it is clear that the observed absorption spectrum of the Ni(II)-doped $CsCdBrCl_2$ system is a superposition of the spectra of many species. The $^3A_{2g} \rightarrow {}^1A_{1g}$ transition shows transitions of all species with intensities governed by a statistical distribution of Br^-/Cl^- ions in the bridging halide positions of the $[Cd_3X_{12}]^{6-}$ trimer in a 1:1 ratio. It is demonstrated in Figures 4 and 7 that the energy of this transition is much more sensitive to the inter-electron repulsion parameters than to the ligand field. It has been noted previously[37] that a low C/B ratio and poor agreement between the calculated and experimental energies of the $^3A_{2g} \rightarrow {}^1A_{1g}$ transition are symptomatic of a significant differential nephelauxetic effect arising from covalency differences between the octahedral t_{2g} and e_g orbitals. Since the e_g orbitals are σ-antibonding and the t_{2g} orbitals π-antibonding, the differential nephelauxetic effect will increase with increasing covalency. The e_g orbitals will experience a greater metal−ligand covalency with an increase of Br^- ligands, reducing the inter-electron repulsion relative to the t_{2g} orbitals.

The differential nephelauxetic effect is conveniently parametrized in a scheme introduced by Lohr.[38] Here the two covalency factors f_e and f_t are introduced for octahedral symmetry. These factors reduce the matrix elements of all operators acting on the orbital part of the wave functions. The two-electron inter-electron repulsion integrals are reduced to

$$\langle ij|e^2/r_{12}|k1\rangle = (\alpha A + \beta B + \gamma C)(f_i f_j f_k f_l)^{1/2} \qquad (6)$$

where α, β, and γ are the usual coefficients for the Racah parameters and the f_i's correspond to either f_e or f_t depending on whether i is an e_g or a t_{2g} orbital.

Using the inter-electron repulsion integrals,[21] the expression for the energy of the $^3A_{2g} \rightarrow {}^1A_{1g}$ transition can be found to be

$$E(^3A_{2g} \rightarrow {}^1A_{1g}) = (12B + 2C)f_e^2 + (5B + {}^5/_2C)f_t^2 - \{[(4B + 2C)f_e^2 + (5B + {}^5/_2C)f_t^2 + 2\Delta]^2 + 6(2B + C)^2 f_e^2 f_t^2\}^{1/2} \qquad (7)$$

Neglecting the effect of Δ and assuming $f_e^4 - f_e^2 f_t^2 \ll f_t^4$, the above expression reduces to

$$E(^3A_{2g} \rightarrow {}^1A_{1g}) = (12B + 2C)f_e^2 \qquad (8)$$

The energy difference, ΔE, between two complexes $[NiBr_xCl_{6-x}]^{4-}$ and $[NiBr_xlCl_{7-x}]^{4-}$ ($x = 1$, ..., 6) is then

$$\Delta E(^3A_{2g} \rightarrow {}^1A_{1g}) = (12B + 2C)[f_e(Br_{x-1}Cl_{7-x})^2 - f_e(Br_xCl_{6-x})^2] \qquad (9)$$

The constant $\Delta E = 397$ cm^{-1} observed implies that this energy difference is independent of x. The difference in the square of f_e is of the order of 0.01 using the observed ΔE and the free-ion values in eq 9. It is not clear how the differential nephelauxetic parameters, f_e and f_t, should vary for the mixed $[NiBr_xCl_{6-x}]^{4-}$ complexes. The observation that the difference in the energy of the $^1A_{1g}$ transition shifts as a *linear* function of x implies that f_e^2 rather than f_e varies linearly with x.

The other important consequence of the differential nephelauxetic effect relevant to the present study concerns the fit of the ligand-field calculations in general. As pointed out by Stranger,[37] increasing covalency in a six-coordinate complex lowers the effective cubic ligand-field splitting:

$$E(^3A_{2g} \rightarrow {}^3T_{2g}) = \Delta + 8B(f_e^2 - f_e f_t) \qquad (10)$$

Upon going from $[NiCl_6]^{4-}$ to $[NiBr_6]^{4-}$, the ligand field, Δ, is expected to increase, but the covalency is also expected to increase. The increased covalency causes f_e to decrease, so that $E(^3A_{2g} \rightarrow {}^3T_{2g})$ decreases for a fixed value of Δ. The observed $E(^3A_{2g} \rightarrow {}^3T_{2g})$ is then a balance of these two effects. If these two effects are not considered together, one can erroneously come to the conclusion that Δ decreases from $[NiCl_6]^{4-}$ to $[NiBr_6]^{4-}$. The normal ligand-field calculation using B and C cannot account for the experimentally observed ordering in the $^3A_{2g} \rightarrow {}^1T_{2g}$, $^1A_{1g}$ states of Ni(II)-doped $CsCdBrCl_2$ and

(37) Stranger, R.; McMahon, K. L.; Gahan, L. R.; Bruce, J. I.; Hambley, T. W. *Inorg. Chem.* **1997**, *36*, 3466−3475.

(38) Lohr, L. L. *J. Chem. Phys.* **1966**, *45*, 3611−3622.

$CsCdBr_3$. Figure 8 summarizes the trends in (a) the differential nephelauxetic parameters and (b) the calculated excited-state energies. The trends in f_e, f_t, and Δ derived from the fits to the experimental energy level structure in Ni(II):$CsCdBrCl_2$ nicely reproduced the relationships expressed in eq 10. Replacing Cl^- ions with Br^- ions in the Ni(II) coordination sphere leads to a decrease in f_e, with a nearly perfect linear decrease in f_e^2, a slight increase in f_t, and an increase in Δ. The calculated energy of the $^3A_{2g} \rightarrow {}^1A_{1g}$ transition and the energy ordering of the $^1T_{2g}$, $^1A_{1g}$ excited states are in very good agreement with the experimental observations. Comparison to the parameters of the pure compounds shown at the sides of Figure 7 shows that an extrapolation from the mixed-halide compound and to the pure-halide compounds is only partly possible, as already discussed.

In contrast to the differential nephelauxetic model, the normal ligand-field approach is considerably less successful in describing the energies and the order of the $^3A_{2g} \rightarrow {}^1T_{2g}$, $^1A_{1g}$ transitions. On average, the $^1A_{1g}$ state is calculated more than 500 cm^{-1} too high in energy, clearly a poorer result than that of the calculation using the differential nephelauxetic model, where the $^1A_{1g}$ state is calculated only about 60 cm^{-1} too low in energy compared to the experimentally assigned energies. Fitting the $^3A_{2g} \rightarrow {}^1A_{1g}$ transition for the different $[NiBr_xCl_{6-x}]^{4-}$ isomers gives the expected increases in the *B* and *C* parameter values but reduces Δ, opposite the expected trend. We have discussed this discrepancy, which is also obvious from the calculations on the pure compounds above.

Investigation of the $^3A_{2g} \rightarrow {}^3T_{1g}$(F), ^1E_g Spectral Region. The Ni(II) halide $^3A_{2g} \rightarrow {}^3T_{1g}$(F), ^1E_g absorption bands have been considerably discussed in the literature and a number of models have been proposed for understanding this spectral range.[5,37,39,40] Unlike the $^3A_{2g} \rightarrow {}^1T_{2g}$, $^1A_{1g}$ transitions, those around 11 000 cm^{-1} are less well resolved, making a detailed analysis difficult. For the assignment of the excited states, assuming Ni(II) in approximate O_h symmetry, we utilized the comparison of Ni(II):$CsCdBrCl_2$ with the pure halide hosts $CsCdBr_3$ and $CsCdCl_3$ (see Figure 2) and followed the work of Bussière and Reber.[40] According to their model, the vibronic progression on the high-energy side of the $^3A_{2g} \rightarrow {}^3T_{1g}$(F), ^1E_g band with a characteristic separation energy *larger* than the a_{1g} vibrational energy of the compound can be assigned to the excited state with predominant singlet character. This increase in the vibrational energy is due this state being the upper of two coupled states, which causes an effective increase in the force constant of the potential energy surface.[40] For the lower of the coupled surfaces, the energy of the a_{1g} vibration is expected to be reduced.

The $^3A_{2g} \rightarrow {}^3T_{1g}$(F), ^1E_g transitions of Ni(II):$CsCdBr_3$ are characterized by two relatively weak, sharp features on both sides of an intense, broad band centered around 11 200 cm^{-1}. The weak transition around 11 700 cm^{-1} faintly shows a vibrational structure with a separation energy of 187 cm^{-1}, close to the a_{1g} local vibration mode of 185 cm^{-1} estimated for $[NiBr_6]^{4-}$ in $CsCdBr_3$ (Figure 2). This progression is seen more clearly in absorption and MCD experiments at 1.6 K (not shown here). At 1.6 K, the other weak feature at 10 600 cm^{-1} shows vibrational structure with an energy separation of 134 cm^{-1}, as well as the broad background. We identify the lower and upper peaks at 10 600 and 11 700 cm^{-1} as those for transitions to the coupled Γ_3 spin−orbit states with mainly ^1E_g character and $^3T_{1g}$ character, respectively. The reduction in the a_{1g} vibrational frequency in the progression based on the lower peak is then due to the softening of the lower potential surface involved in the coupling. On the other hand, the reduction in the a_{1g} vibrational frequency in the progression on the broad background may be due to the increased antibonding character of the $^3T_{1g}$ state as a consequence of the $t_{2g}^5e_g^3$ electron configuration.

For Ni(II):$CsCdCl_3$, the $^3A_{2g} \rightarrow {}^3T_{1g}$(F), ^1E_g transitions show a broad, unstructured band centered at 10 750 cm^{-1} and a vibrational progression around 12 700 cm^{-1}, with a separation of 282 cm^{-1}. This energy is *higher* than the a_{1g} local vibration mode for $[NiCl_6]^{4-}$ in $CsCdCl_3$ (264 cm^{-1}).[36] This is due to the steeper potential walls resulting from the coupling of the ^1E_g and $^3T_{1g}$ states as observed for Ni(II):$CsMgCl_3$.[40] In the Ni(II):$CsCdCl_3$ case, we identify the peak at 12 700 cm^{-1} as that for a transition to a state of predominantly ^1E_g character. With a shoulder on the low-energy side of the broad band centered around 11 400 cm^{-1} and some features of an unresolved vibrational progression on the high-energy side, Ni(II):$CsCdBrCl_2$ shows an intermediate situation between the pure systems (Figure 2). From the calculations using the differential nephelauxetic approach (Figure 8), it is expected that substitution of Cl^- with Br^- has an effect on the energy of the $^3A_{2g} \rightarrow {}^1E_g$ transition comparable to that calculated and experimentally observed for the $^3A_{2g} \rightarrow {}^1A_{1g}$ transition.

Conclusions

$CsCdBrCl_2$ is a novel host material, an example of a mixed-halide compound, which has been structurally characterized by X-ray diffraction and optical spectroscopy using the Ni(II) ion as a probe. The structure of $CsCdBrCl_2$ was shown to consist of comer-sharing $[Cd_3X_{12}]^{6-}$ trimers. Each trimer has a structure of three face-sharing $Cl_3CdX_3CdX_3CdCl_3$ octahedra where X has equal probability of being a Br^- or Cl^- ion. This equal occupancy of the bridging halide positions occurs over the whole crystal rather than within each $[Cd_3X_{12}]^{6-}$ trimer unit. Within the crystal, all seven types of the mixed-halide $[CdBr_xCl_{6-x}]^{4-}$ ($x = 0, ..., 6$) coordinations exist.

The energy of the $^3A_{2g} \rightarrow {}^1A_{1g}$ transition in the $[NiBr_xCl_{6-x}]^{4-}$ species is a *linear* function of *x*. An inhomogeneous broadening results from the halide disorder and is evident on two levels. There is a disorder determined by the *number* of Br^- and Cl^- ligands, which results in the $^3A_{2g} \rightarrow {}^1A_{1g}$ transition varying over 2750 cm^{-1}. There is also a disorder determined by the *position* of Br^- and Cl^- ligands, leading the superposition of $^3A_{2g} \rightarrow {}^1A^{1g}$ transitions due to different ligand fields from the 29 possible nonequivalent structural isomers. This disorder results in an ~100 cm^{-1} spread of the energy of the $^3A_{2g} \rightarrow {}^1A_{1g}$ transition; the transitions of the individual structural isomers are unresolved in the present case. The energy of the $^3A_{2g} \rightarrow {}^1A_{1g}$ transition is principally determined by the variation in the inter-electron repulsion rather than the ligand field.

In the past few years, many theoretical studies using density functional theory have been devoted to gaining a more fundamental understanding of the trends due to chemical variation in transition-metal and rare-earth-metal compounds. Most of these studies concentrated on the differences in chemical bonding and spectroscopic properties upon substitution of the metal center. Less work has investigated the nephelauxetic effect due to substitution of the ligands. A recent density functional study on Co(III) complexes reproduces and explains the experimentally found observations of the nephelauxetic effect

(39) Solomon, E. I.; Ballhausen, C. J. *Mol. Phys.* **1975**, *29*, 279−299.
(40) Bussière, G.; Reber, Ch. *J. Am. Chem. Soc.* **1998**, *120*, 6306−6315.
(41) Chan, J. C. C.; Wilson, P. J.; Au-Yeung, C. F.; Webb, G. A. *J. Phys. Chem. A* **1997**, *101*, 4196−4201.

due to variation of the ligands.[41] Chemical variation is known as an important and powerful tool to tune the spectroscopic properties of optical compounds. From the present study of the mixed $[NiBr_xCl_{6-x}]^{4-}$ system, we can predict that the energy of the excited-state transition $^3T_{2g} \rightarrow {}^1A_{1g}$ involved in the excitation avalanche can be varied between 12 500 and 14 250 cm^{-1} on going from the pure $[NiBr_6]^{4-}$ complex to the pure $[NiCl_6]^{4-}$ complex, respectively.

Because of its interesting crystal structure, built of face-sharing $[Cd_3X_{12}]^{6-}$ (X = Br, Cl) units, $CsCdBrCl_2$ could be an interesting compound for the incorporation of trivalent metal ions. Well-defined pairs $M^{3+}-V-M^{3+}$ and $M^{3+}-M^{3+}-V$ (V = vacancy) are expected to form, allowing for a strong interaction between the active centers, due to the small Cd−Cd distance of 3.327 Å within the face-sharing $[CdX_6]^{4-}$ octahedra. Additionally, this compound offers the rare opportunity to study the effect of a random distribution of Cl^- and Br^- ions in bridging halide positions on the spectroscopic properties of the incorporated dopant ions. Chemical substitution along the halide series offers a way to study the well-known trends along the spectrochemical and nephelauxetic series. Superficially it appears that the mixed-halide $[NiBr_xCl_{6-x}]^{4-}$ complexes in Ni(II):$CsCdBrCl_2$ do not fit into these series. However, if the differential nephelauxetic effect is taken into account, good agreement is found between the experimental and the calculated energy level structures.

Acknowledgment. Financial support for this research was provided by the Swiss National Science Foundation and the Australian Research Council. We gratefully acknowledge N. Furer and H. U. Güdel (Universität Bern, Switzerland) for assistance with the crystal growth, P. V. Bernhardt (University of Queensland, Australia) for the crystal structure determinations, E. R. Krausz (Australian National University) for absorption and luminescence experiments, G. Foran and J. Lester, (Australian National Beam Facility, Tsukuba, Japan) for the EXAFS experiments, and N. Calos (University of Queensland, Australia) for assistance with the EXAFS analysis.

Supporting Information Available: Listings of energy level calculation parameters for Ni(II) in different halide host materials, Ni(II)−halogen bond lengths, and results of differential nephelauxetic ligand-field calculations, as well as EXAFS spectra of the Ni(II)-doped $CsCdBr_3$, $CsCdBrCl_2$, and $CsCdCl_3$ systems. This material is available free of charge via the Internet at http://pubs.acs.org.

IC000899L